Translational and nontranslational motion of perturbed Turing patterns

Vladimir K. Vanag and Irving R. Epstein
Department of Chemistry and Volen Center for Complex Systems, MS 015, Brandeis University, Waltham, Massachusetts 02454-9110, USA

(Received 26 December 2002; published 27 June 2003)

When the front and rear boundaries of a Turing pattern with nonzero flux boundary conditions move synchronously, several modes of motion of the pattern are found. Traveling boundaries can be obtained experimentally by illuminating a Turing-unstable system through a moving mask consisting of a single dark stripe with a light intensity sufficient to suppress pattern formation. All structured moving patterns belong to two general types: smooth translation at low mask velocity v_x and nontranslational (''hopping'') at intermediate v_x. At high v_x, Turing patterns are unable to form, and an unstructured striped image of the mask is seen. When the mask width exceeds the Turing wavelength, bistability between different types of moving patterns can occur as v_x is varied.

DOI: 10.1103/PhysRevE.67.066219 PACS number(s): 82.40.Ck, 47.54.+r

I. INTRODUCTION

Turing patterns and motion would seem, at first glance, to be incompatible phenomena. However, under some conditions, moving Turing patterns are possible. We recently found [1] in the Belousov-Zhabotinsky (BZ) reaction dispersed in an aerosol OT water-in-oil microemulsion (BZ-AOT system) the existence of dash waves, which consist of parallel lines of propagating spots or dashes. We showed experimentally and in model simulations that when the microemulsion has a bimodal distribution of water nanodroplets with two different droplet radii (2.1 and 20 nm), the BZ-AOT system has two steady states, one of which exhibits excitability and the other possesses a pseudo-Turing instability. The excitable state generates trigger waves that can switch the system in the area occupied by waves to the pseudo-Turing unstable steady state, which can result in the trigger wave splitting into fragments or dashes separated by gaps. Each dash wave may be thought of as a one-dimensional propagating Turing structure with characteristic wavelength (gap+dash) $2\pi/\mathbf{k}_0$, where $\mathbf{k}_0$ is the wave number corresponding to the pseudo-Turing instability.

Moving spots (the analog of dash waves) have also been obtained recently in a very different experiment involving external perturbation of Turing patterns in the chlorine dioxide–iodine–malonic acid (CDIMA) reaction [2]. Striped Turing patterns were illuminated through a striped mask oriented parallel to the pattern with the same spatial periodicity of dark and transparent zones. Light passing through the transparent regions of the mask suppresses pattern formation [3], so that Turing structures can survive only in the dark zones. When the mask is slowly moved perpendicular to the stripes, the Turing patterns move with the mask. At a critical mask velocity, the Turing stripes split into a linear array of spots moving coherently in the same direction. Further increase of v_x leads to a ripple structure. This symmetry-breaking phenomenon is not yet understood.

These two experiments have much in common and inspired us to investigate the relationship between Turing structures and traveling boundaries (mask motion). The latter is equivalent, in a sense, to the propagation of a pair of trigger waves. As the mask starts to move, say, toward the right, the left edges of a striped Turing pattern are brought under illumination and are suppressed, while new shadow zones become available for expansion of Turing patterns to the right. The right border of each Turing stripe represents a kind of trigger wave front, since the system there is switched abruptly from one state (the suppressed state under illumination) to another (the excited dark state). The left border of each Turing stripe corresponds to a trigger wave front with the opposite switching.

Illumination of Turing patterns through a moving mask has a close relation with three types of experiments that have recently been performed: (1) illumination of Turing patterns through stationary masks of different wavelengths [4]; (2) spatially uniform, time-periodic illumination of Turing patterns [3,5]; and (3) formation of Turing structures in the presence of a moving region of illumination [6].

In this paper we study the dependence of Turing patterns on the velocity of a one-stripe moving mask in a broad range of mask velocities, mask widths, and light intensities. In Sec. II we outline our model and explain our choice of parameters for the Turing patterns under investigation. In Sec. III we present the results of our numerical simulations for a two-dimensional system. In Sec. IV we analyze the transition from translational to nontranslational motion for the one-dimensional case. Section V contains our discussion and conclusions.

II. A MODEL: PRELIMINARY RESULTS FOR A STATIONARY MASK

To simulate Turing patterns, we employ the well-known Lengyel-Epstein model [Eqs. (1) and (2)] for the CDIMA reaction [7] augmented by an additional term w that characterizes the light intensity [3,4]

$$\partial u/\partial t = a - u - 4uv/(1+u^2) - w(x,t) + \Delta u, \qquad (1)$$

$$\partial v/\partial t = \sigma b[u - uv(1+u^2) + w(x,t)] + \sigma d\Delta v. \qquad (2)$$

The variables u and v are the dimensionless concentrations of $[I^-]$ and $[ClO_2^-]$, respectively; a,b,d (the ratio of the

diffusion coefficients of u and v), and σ are dimensionless parameters that involve the reaction rates and input concentrations of the major chemical species. The rate of the photochemical reaction $w(x,t)$ is a function of the spatial coordinate x and time t and is expressed as

$$w(x,t)=w_1+w_2 m,$$

where $m=1$ if $x<x_m$ or $x>x_m+l_m$, and 0, if $x_m<x<x_m+l_m$; $x_m=x_0-v_x l$, where v_x is the velocity of the moving mask in the x direction, and x_0 is the initial x coordinate of the left edge of the mask stripe of width l_m.

Equations (1) and (2) were solved numerically with the FLEXPDE package [8] with periodic boundary conditions for the left and right borders of a rectangular area 30×30 in size (in some cases, with very wide stripes, we employ a 40×30 area; for one-dimensional simulations we used a segment as long as 150). Zero flux boundary conditions were used at the top and bottom of the area. FLEXPDE refines the triangular finite element mesh until the estimated error in any variable is less than a specified tolerance, which we chose as 10^{-4}, at every cell of the mesh.

We choose the parameters w_1 and w_2 so that the system (1), (2) has a stable homogeneous steady state at $w=w_1+w_2$ (both eigenvalues are negative at all wave numbers $\mathbf{k}$), while at $w=w_1$, the system possesses one positive real eigenvalue in the range $0<\mathbf{k}_{\min}\leqslant\mathbf{k}\leqslant\mathbf{k}_{\max}$. The system (1), (2) then has a Turing instability at $w=w_1$. For a well-chosen set of parameters a, b, σ, and d, we can obtain all types of Turing patterns [Fig. 1(a)] by varying w_1 [9].

As Fig. 1(a) shows, white spots appear at low values of w, stripes at intermediate w, and black spots at higher w. When $w>5.786$, only the uniform steady state is stable. Therefore, we use $w_1+w_2=6$ to suppress Turing patterns [since the steady state of model (1), (2) is $u_{SS}=a/5-w$, we must have $w<a/5$; for the parameters used here, $a/5=7.2$]. Bistability between stripes and black spots is found when w is between about 3.5 and 5. The type of pattern that occurs in the dark zone of the mask, where $w=w_1$, depends upon both w_1 and the width l_m of the mask. Figures 1(b) and 1(c) show that the bistability region vanishes when $l_m<\lambda_T$ [λ_T is the Turing wavelength obtained by linear stability analysis of the system (1), (2), $\lambda_T\cong4.2$–4.5 at $w=4$–4.5], and reappears for $l_m\geqslant\lambda_T$.

Comparison of Figs. 1(b) and 1(c) at $w_1=0$ with the Turing patterns in Fig. 1(a) at $w=0$ reveals that the white spot Turing pattern disappears if l_m is too small. This phenomenon has a straightforward interpretation. The regions covered by the mask in Figs. 1(b) and 1(c) have special boundary conditions at their left and right boundaries (flux to and from the illuminated homogeneous steady state), while the patterns in Fig. 1(a) have zero flux or periodic boundary conditions. The special boundary conditions in Figs. 1(b) and 1(c) correspond to a "white background," where $w=w_1+w_2$. White spot Turing patterns at $w=0$ have a "black background," and are incompatible with a "white background." Since the width of the dark area is less than a Turing wavelength ($\lambda_T\cong5.6$ at $w=0$), there is not enough room to fit both the "proper" background and a set of white spots, so instead the system generates a black stripe at $w_1=0$.

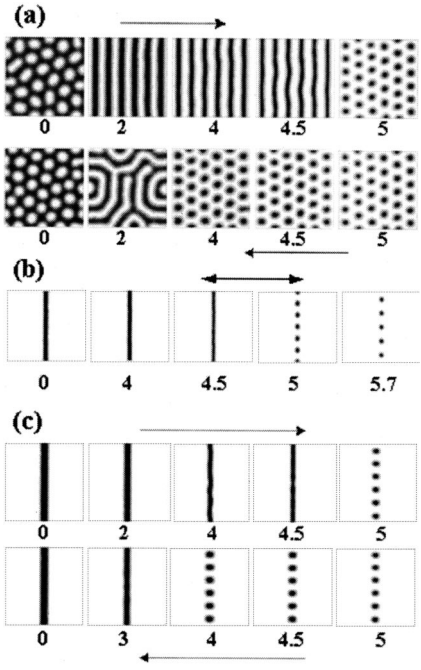

FIG. 1. Turing patterns in model (1), (2) illuminated through a mask of width l_m=(a) 30, (b) 2, (c) 4.6 for $a=36$, $b=2.8$, $d=1.2$, and $\sigma=30$. Size=30×30. Arrows show directions of changing w_1 (numbers below snapshots). In (a) and (c), upper (lower) arrow shows direction of changing w_1 for upper (lower) row of patterns. (a) $l_m=30$=size and $w=w_1$. For $w_1=2$ in the upper row of each set of patterns, an initially homogeneous steady state was perturbed on a narrow stripe at the left boundary. The rest of the upper row was generated by starting from the Turing pattern found at one value of w_1 and then increasing w_1 to the next value shown. The lower row of patterns was generated by starting from the pattern at $w_1=5$ and decreasing w_1 in the reverse of the process described above. If the initial pattern is that obtained at $w_1=0$, the pattern found at $w_1=2$ is the one in the lower row. (b), (c) Intensity of light w inside mask stripe is w_1; $w=w_2+w_1=6$ outside this stripe.

In Fig. 2 we examine how the type of Turing pattern varies with l_m at several w_1. For $w_1=0$ and 4 (as well as for $w_1=4.5$, not shown), there are regions of l_m where the pattern found depends on the initial conditions. Since we obtained bistability at $w=4$ and 4.5 on varying w without a mask [Fig. 1(a)], it is not surprising to find bistability with respect to l_m for these values of w_1. We also anticipate the lack of bistability with respect to l_m found at $w_1=2$ and 5.2, since these levels of illumination do not yield bistability when w is varied. The unexpected bistability at $w_1=0$ [columns (a) and (b) in Fig. 2] appears to be associated with stabilization of the stripe pattern, which emerges faster than the spot pattern, by the white background of the illuminated region. Thus, if we start with homogeneous initial conditions or the stripe pattern, the latter can persist ($l_m=8,11.2$), or at least linger in the form of linked spots ($l_m=12.6$), though if we start from the natural white spot pattern, it remains stable so long as $l_m\geqslant\lambda_T$.

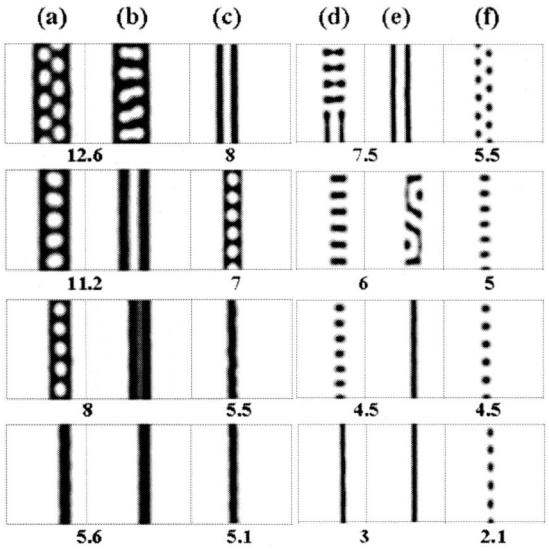

FIG. 2. Stationary Turing patterns illuminated through a mask of width l_m (numbers below snapshots). Inside mask stripe, intensity of light $w_1=0$ for columns (a) and (b), 2 for (c), 4 for (d) and (e), and 5.2 for (f); $w=w_1+w_2=6$ outside this stripe. All other parameters as in Fig. 1. Patterns in columns (b) and (e) are obtained from homogeneous steady state as the initial pattern. Patterns with larger l_m were used as initial conditions for patterns in columns (a) and (d). No bistability regions are found for $w_1=2$ [column (c)] and $w_1=5.2$ [column (f)].

Understanding how the Turing patterns change with l_m will be important later in interpreting the behavior of moving Turing patterns as a function of mask velocity v_x. Our preliminary calculations at $v_x=0$ allow us to find representative values of w_1 and l_m, which we use in our study of the moving mask. We choose $w_1=5.2$ for black-spot Turing patterns, $w_1=4$ and 4.5 for bistability, $w_1=2$ for striped Turing patterns, and $w_1=0$ for white-spot patterns. We will also consider the effect of varying l_m ($l_m<\lambda_T$, $l_m\cong\lambda_T$, and $l_m\cong 2\lambda_T$).

Our analysis of the behavior of a moving mask requires knowledge of the rate of Turing pattern expansion into a region where $w=w_1$. To obtain these data, we performed computer experiments analogous to those made by Kaern *et al.* [6] or Jensen *et al.* [10], but in two dimensions. A rectangular area 50×20 in size is divided into two regions. The right part (10×20) is illuminated with $w=6$, and the left part (40×20) with $w=w_1$. Turing patterns start to appear at the boundary between the parts and spread to the left. For $w_1=2$, 4, and 4.5, stripes emerge one by one [Fig. 3(a)]; for $w_1=0$, columns of white spots emerge and propagate in tandem with intervening black stripes. For $w_1=5.2$, stripes appear first and then are transformed into black spots. In this case [Fig. 3(b)] we calculate two rates of pattern propagation, one for stripes and another for spots. These rates of frontal propagation V_{intr} are summarized in Table I.

Note that in the reverse process, in which Turing patterns initially occupy the entire area with $w=w_1$ and then the light intensity is instantaneously increased to $w=6$ in most of the area, while the smaller part remains at $w=w_1$, no propagating front of pattern disappearance is found. Instead, all Turing peaks disappear simultaneously after a characteristic time between 0.2 and 0.8 depending on the initial type of pattern.

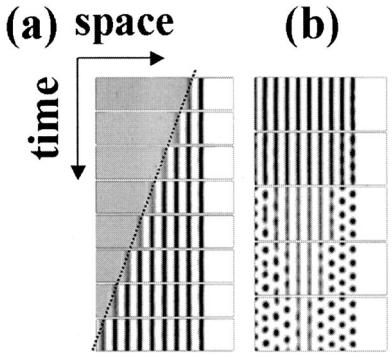

FIG. 3. Turing patterns spreading for $w_1=$(a) 4.5 and (b) 5.2. Right rectangular area (10×20) is illuminated at $w=6$; left rectangular area (40×20) is illuminated at $w=w_1$. Time intervals between snapshots are $\Delta t=1$ for (a) and 5 for (b). In (b), the first snapshot is taken at $t=10$, after the striped pattern has spread throughout the left area. The slope of the dashed line in (a) determines the rate of a stripe pattern's expansion, V_{intr}.

III. MOVING MASK

We carried out simulations of moving masks at a variety of mask velocities and lengths. Representative results of our simulations are presented in Tables II (values of w_1 for which only one type of Turing pattern is found) and III (values of w_1 in a bistable region of Turing patterns) and in Fig. 4. We find three general types of pattern movement: (i) smooth translational movement at small velocities, where Turing patterns follow the moving mask while maintaining their structure; (ii) nontranslational movement at moderate velocities, where patterns periodically change their structure; and (iii) translational movement of a single unstructured stripe at high velocities. In this last, and least interesting, case, the moving stripe may be viewed as the shadow of the moving mask. These stripes are seen in the bottom rows of Tables II and III below the single bold separation line. The critical velocities $v_{\text{cr un}}$ at $l_m=2\lambda_T$, for which this uniform stripe emerges, are given as a function of w_1 in the right column of Table I. The striking agreement between $v_{\text{cr un}}$ and V_{intr} suggests that the appearance of these unstructured stripes is related to the rate of pattern formation in a uniform medium. If $v_x>V_{\text{intr}}$, then Turing patterns do not have suf-

TABLE I. Rate V_{intr} of Turing pattern expansion and critical velocity $v_{\text{cr un}}$ for onset of a uniform stripe propagating pattern as functions of light intensity w_1.

w_1	V_{intr}	$v_{\text{cr un}}$
0	1.3	1.5
2	2.6	2.5
4	4.7	4.4
4.5	4.5	4–5
5.2	4.4 (stripes) 0.8 (spots)	4–5

TABLE II. Typical patterns at velocity v_x for a mask of width l_m at $w_1=5.2$ and 2. Note that at any v_x, only stripe patterns occur at $l_m=4.5$ for $w_1=2$ ($\lambda_T=5.03$) and at $l_m=5.6$ for $w_1=0$ ($\lambda_T=5.61$). (a)–(e) are summations of long series of consecutive snapshots with a short time interval between them; other patterns are single snapshots. Nontranslational motion for cases (a), (b), and (e) are shown in Fig. 4. Individual snapshots for cases (c) and (d) are analogous to those shown in Figs. 4(c) and 4(d), respectively.

v_x	$w_1=5.2$	v_x	$w_1=2$ [a]
0 – 0.5 $l_m=4.5$ [b]		0 – 0.17 $l_m=5.5$ [c]	
1.1 - 1.2 $l_m=1$		0.16 – 0.22 $l_m=10.5$	
0.3 – 0.5 (a), $l_m=8.1$		0.22 – 0.3 (e), $l_m=5.5$	
0.6 – 1.3 (b), $l_m=4.5$		0.4 – 1 (c), $l_m=5.5$ [d]	
1.45 – 3 (d), $l_m=4.5$		1.2 – 2.2 $l_m=10.5$	
($l_m=1$) 1.3 – ($l_m=4.5$) 4 – ($l_m=8.1$) 5 -		($l_m=5.5$) 1.2 - ($l_m=10.5$) 2.5 –	

[a]Pattern at $w_1=0$ and $l_m=2\lambda_T$ is analogous to that at $w_1=2$ and $l_m\cong 2\lambda_T$ with the exception that bistability is found for $v_x=0-0.2$.

[b]$\lambda_T=4.05$ at $w_1=5.2$.

[c]Translational two-stripe pattern for $l_m=10.5$ is found at $v_x=0-0.15$.

[d]Analogous white hexagon summation patterns are found for $l_m=10.5$ at $v_x=0.26-2$.

ficient time to develop in the dark region (if the width of this region does not significantly exceed λ_T), and only a shadow of the mask is seen. We will discuss the dependence of the width of the unstructured propagating stripe on v_x in Sec. IV.

The most interesting motions are types (i) and (ii). Each consists of several subtypes. In general, there are two different types of nontranslational pattern motion; these are presented in Tables II and III between the hatched and the bold separation lines. We call these behaviors hexagonal motion [cases (b) and (c) of Table II and case (c) of Table III] and striped motion [case (d) of Table II, for example], because of their similarity with hexagonal-spot and striped Turing patterns. Although individual snapshots of hexagonal motion do not exhibit hexagonal-spot patterns [see Figs. 4(b) and 4(c)], superposition of a sequence of snapshots with a short time interval between them reveals the hexagonal pattern. An example of striped motion is shown in Fig. 4(d). For short l_m, the striped pattern periodically alternates between one and two stripes; for longer l_m, between two and three stripes.

For some l_m and w_1 ($l_m=4.5$ at $w_1=4$; $l_m=5.5$ at $w_1=2$), we observe pure hexagonal nontranslational movement. For other l_m and w_1 ($l_m=4.5$ and $l_m=8.46$ at $w_1=4.5$; $l_m=8.84$ at $w_1=4$), only striped motion is found. In a few cases ($l_m=8.1$ and $l_m=4.5$ at $w_1=5.2$; $l_m=10.5$ at $w_1=2$), both types of nontranslational motion are seen for the same

TABLE III. Typical patterns at velocity v_x for a mask of width l_m at $w_1=4$ and 4.5. Only stripe patterns occur for $l_m=2$ at any v_x. With the exception of (c), each pattern is a single snapshot; (c) is a summation of a long series of consecutive snapshots with a short time interval between them. Typical behavior for cases (c) and (d) is shown in Fig. 4. For $w_1=4.5$ ($\lambda_T=4.23$), bistability is found for $l_m=4.5$ at $v_x=0-0.2$ and at $v_x=0.8-1.1$; and for $l_m=8.46$ at $v_x=0-0.1$ and at $v_x=0.4-1.1$. For $w_1=4$ ($\lambda_T=4.42$), tristability is found for $v_x=0-0.1$, bistability for $v_x=0.1-0.3$, and for $v_x=0.6-0.7$ at $l_m=8.84$, while at $l_m=4.5$, bistability occurs for $v_x=0-0.2$.

v_x	$w_1=4$	v_x	$w_1=4.5$
0 – 0.1 $l_m=8.84$		0 – 0.2 $l_m=4.5$	
0 – 0.3 $l_m=8.84$		0 – 0.25 $l_m=8.46$	
0 – 0.7 $l_m=8.84$		0 – 1.1 $l_m=4.5$	
0.6 – 4.2 $l_m=8.84$		0.4 - 4 $l_m=8.46$	
1.1 – 2.3 (c), $l_m=4.5$		0.8 – 4 (d), $l_m=4.5$	
4.4 -		5 –	

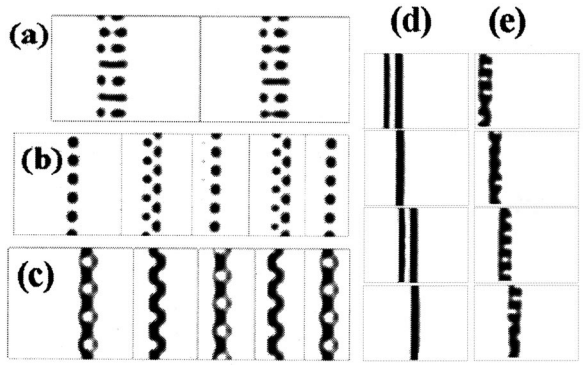

FIG. 4. Examples of nontranslational motion. Sequences of snapshots for cases (a), (b), and (e) correspond to cases (a), (b), and (e) in Table II; $v_x=0.3$ for (a) and (e) and 1 for (b). Time intervals between snapshots are $\Delta t=12$ for (a) and (e), 4.25 for (b). In (b) and (c), only the left snapshot shows the full area; other snapshots omit the uniform white area in the left half of the medium. Sequences of snapshots for cases (c) and (d) correspond to cases (c) and (d) in Table III; (c) $v_x=1.2$, $\Delta t=1.2$; (d) $v_x=2$, $\Delta t=1$.

TABLE IV. Period T of pattern recovery (hopping) for nontranslational motion at velocity v_x of a mask of width $l_m=4.5$ at two values of light intensity w_1 for 2D and 1D cases. Top group, $w_1=5.2$ ($\lambda_T=4.05$), 2D; middle group, $w_1=4.5$ ($\lambda_T=4.23$), 2D; bottom group, $w_1=5.2$, 1D. $v_{cr}\approx 0.5-0.55$ for the top 2D case. v_{cr} cannot be found for the middle group due to bistability between $v_x=0.8$ and 1.1 (see Table III).

v_x	T	$v_x\times T$	$(v_x\times T)/\lambda_T$
1	8.2	8.2	2.02
1.2	6.7	8.04	1.98
1.3	6.3	8.19	2.02
1.45	2.8	4.06	1
2	2	4	0.99
3	1.35	4.05	1
1.3	3.25	4.23	1
1.5	2.83	4.24	1
2	2.075	4.15	0.98
2.5	1.69	4.23	1
3	1.4	4.2	0.99
4	1.05	4.2	0.99
0.155	∞		
0.1565	129	20.19	4.98
0.158	110	17.38	4.29
0.1595	100	15.95	3.94
0.162	70.6	11.4	2.82
0.165	58	9.87	2.36
0.17	51.3	8.72	2.15
0.18	37.6	6.76	1.67
0.2	28.6	5.70	1.41
0.3	14.8	4.44	1.1
0.5	8.15	4.07	1.01
1	4	4	0.99
2	2	4	0.99

mask at different v_x. For these cases, hexagonal movement occurs at smaller v_x and striped movement at larger v_x, although for $w_1=2$, bistability between striped and hexagonal motion is found in the range $1.2<v_x<2$. For $w_1=5.2$, the emergence of hexagonal motion at lower mask velocities than striped motion arises from the different rates of expansion of stripes and spots (see Fig. 3 and last row of Table I). Spots propagate much more slowly than stripes, but spots are more stable at $w_1=5.2$ (Fig. 1). When the mask moves relatively slowly, there is enough time for spots to develop. When the mask moves faster, there is insufficient time for spots to mature, and ''unstable'' stripes become stable, in a fashion resembling the generation of a less stable product in a chemical reaction by kinetic as opposed to thermodynamic control.

Nontranslational motion is characterized by a period T for a given pattern to reappear at a distance v_xT beyond its original location. The dependence of T on v_x is presented in Table IV. We observe that the product of T and v_x is equal to $2\lambda_T$ for hexagonal motion and to λ_T for striped motion, so long as v_x is relatively far from the critical velocity of the translational-nontranslational (T-NT) transition.

It is important to note that in nontranslational motion individual stripes or spots do not move. Instead, new stripes or spots emerge at the front end of the mask and old stripes or spots fade and die at the rear end, as if the rearmost object(s) had hopped over or leapfrogged the rest of the pattern to reappear at the front. In translational motion (at smaller v_x) in contrast, the same structure persists at all times, and there is no associated period T for the regeneration of a pattern, but rather a continuous movement of the entire pattern. For some cases close to the T-NT transition, such as those in Table II [cases (a) and (e)], we find an intermediate type of motion, which resembles the movement of an amoeba. In this mode, illustrated in Figs. 4(a) and 4(e), patterns flow by fits and starts into a new position by changing their shapes, e.g., spots become dumbbells, and vice versa.

There are two primary types of translational motion at small v_x: movement of a stripe (or of parallel stripes at larger l_m) and movement of spots (or of multiple columns of spots at larger l_m). Hybrid spot-stripe patterns can also occur (Table II: $l_m=1$, $v_x=1.1-1.2$, $w_1=5.2$; Table III: $l_m=8.84$, $w_1=4$, $v_x=0-0.3$). Translational motion of spots is analogous to the dash waves found in the BZ-AOT system [1].

Bistability between moving stripes and moving spots occurs over a large range of v_x for those parameters for which bistability is found at $v_x=0$ with respect to either w_1 or l_m. For $w_1=4$, $l_m=8.84$ (Table III), we even found tristability among two-stripe ($v_x=0-0.1$), stripe-spot ($v_x=0-0.3$), and dumbbell ($v_x=0-0.7$) patterns for $v_x=0-0.1$. The transition from stripe-translational to spot-translational motion, which was found in experiment [2], occurs at fairly small v_x (about 0.1–0.2) in the bistability range of w_1 ($w_1=4-4.5$). It is likely that this transition is related to instabilities of the moving front.

Qualitatively speaking, the transitions between modes at different v_x are related to the transitions that occur at $v_x=0$ as l_m is varied. Single-stripe, spot, and two-stripe patterns succeed each other as l_m grows [columns (d) and (e) of Fig. 2]. An analogous sequence of patterns is found for the bistable region of w_1 ($l_m=4.5$ and $w_1=4.5$) when v_x increases. A single column of spots at small l_m [Fig. 2(f)] or spot-translational motion at low v_x for $w_1=5.2$ (Table II) is replaced by a hexagonally oriented pair of spot columns at larger l_m or by hexagonal motion at larger v_x, respectively. Intuitively, the two behaviors parallel one another because the width of the perturbed zone, where the concentrations u and v are not equal to their stationary, illuminated values at $w=6$ in Eqs. (1) and (2), increases with v_x.

The number of modes of behavior for moving Turing patterns depends strongly on the mask width. For example, for white spots and stripes ($w_1=0-4.5$), only moving (unstructured) stripes can occur for very small l_m ($<\lambda_T$) at any v_x, while moving spots emerge when $l_m\geqslant\lambda_T$. As l_m increases, the number of accessible moving patterns grows. We did not examine masks of width greater than $2\lambda_T$ for the two-dimensional (2D) case. It is evident, however, that at very large l_m there will be no interaction between patterns forming at the front and dying at the rear edges of a moving

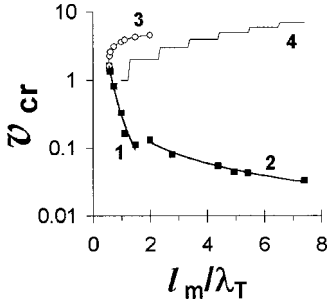

FIG. 5. Dependence of critical mask velocity, v_{cr}, on mask width l_m. Squares are critical velocities for the translational $\rightarrow$nontranslational transition. Circles (curve 3) are critical velocities for the nontranslational$\rightarrow$translational transition. Curve 4 shows number of peaks in a Turing pattern at $v_x=0$. Curves 1 and 2 are fits of the experimental points: $v=0.304(l_m/\lambda_T)^{-2.9617}$ for curve 1 and $0.254(l_m/\lambda_T)^{-1.05}$ for curve 2. Nontranslational motion occurs between curves 3 and 1, 2. λ_T is the Turing wavelength, 4.053 for $w_1=5.2$. All other parameters as in Fig. 1.

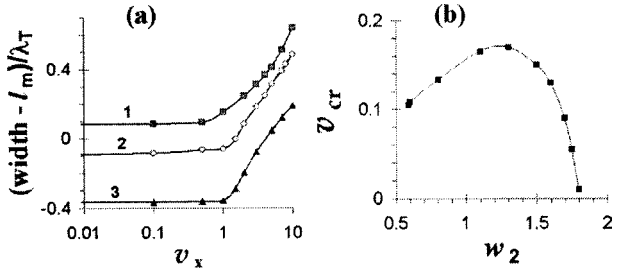

FIG. 6. (a) Dependence of full width at half maximum of the u peak on mask velocity v_x for small l_m (translational motion). $l_m=1$, $w_1=5.2$ for curve 1; $l_m=2$, $w_1=4$ for curve 2; $l_m=4.5$, $w_1=2$ for curve 3. (b) Dependence of critical velocity, v_{cr}, of mask movement on light intensity beyond the mask, $w=w_1+w_2$; $w_1=5.2$, $l_m=8.1$. All other parameters as in Fig. 1.

mask. Thus in the central region of a very wide moving mask we will be limited to the patterns shown in Fig. 1(a) for a stationary mask. We may expect the greatest diversity of moving Turing patterns to occur for moving masks of intermediate width.

IV. TRANSLATIONAL-NONTRANSLATIONAL TRANSITION IN ONE DIMENSION

The translational-nontranslational transition is easier to understand in the 1D case, where we can vary the mask width l_m over a broad range without the need for excessively lengthy simulations. The problem is also simplified by eliminating the distinctions between hexagonal and striped modes of nontranslational motion and between stripe-translational and spot-translational motion.

The values of the critical velocity of the T-NT transition, v_{cr}, obtained by direct computer simulation are presented in Fig. 5. Note that the critical velocities for the T-NT transition are smaller in the 1D than in the 2D case (see also Table IV). With narrow masks that can support only a single peak in the Turing pattern ($l_m/\lambda_T<1.5$, curve 1), the critical velocity varies roughly as l_m^{-3}. For larger l_m (curve 2), we find $v_{cr} \cong l_m^{-1}$.

Figure 5 also shows the l_m dependence (curve 3) of the critical velocity for the transition from nontranslational motion of Turing patterns to translational motion of the unstructured mask shadow. Only the data for $l_m/\lambda_T<2$ are shown. For broader masks, it is difficult to define the unstructured band unambiguously, since the front part of the band resembles the unstructured band seen with narrow masks, while the rear part has enough time to develop incipient Turing structures.

The intersection of curves 1 and 3 in Fig. 5 gives the point to the left of which only translational motion is found at any v_x. Even for this case, a transition between two different translational motions can be found. If we measure the width of the single peak [the width of the u peak at half maximum is shown in Fig. 6(a)], we find that at small v_x the width of a peak is approximately equal to the width of a Turing peak and is essentially independent of v_x. Above a critical velocity, the width of the peak starts to increase with v_x and the amplitude of the peak (not shown) simultaneously begins to decrease.

The dependence of v_{cr} on l_m indicates that processes at the edges of the mask, and consequently the boundary conditions, must affect the T-NT transition. Figure 6(b) shows the dependence of v_{cr} on w_2, the light intensity determining the steady state values of u and v in the homogeneous region beyond the mask. These values of u and v determine the flux boundary conditions.

The problem analyzed here of Turing pattern illumination through a moving one-stripe mask is equivalent to that of a quasi-two-dimensional layer of a reactive mixture at steady state flowing across a fixed striped region, perpendicular to the direction of motion, in which one or more system parameters takes a value that enables the system to exhibit Turing instability. To study translational motion of patterns, one can introduce a moving frame $r=x-v_xt$, or, more generally, one can assume that concentration profiles are of the form $c(x,t)=c_T(r)e^{i\omega t}$ with non-zero-flux boundary conditions at the stripe borders. Such a substitution introduces convective terms of the form $v_x(1+i\omega)\partial c_T/\partial r$. In general, solutions will exist with $\omega=0$ for $v_x<v_{cr}$, corresponding to stationary patterns. If v_x exceeds the critical velocity v_{cr}, we have $\omega \neq 0$, and the solution corresponds to nontranslational motion.

Nontranslational motion in the moving frame actually represents waves, which usually emerge in the case of the wave instability [sometimes called the finite wavelength instability, and characterized by a positive real part Re(λ) and nonzero imaginary part Im(λ) of the largest eigenvalue, for some range of wave numbers k, $0<k_1<k<k_2$]. To demonstrate that Turing patterns transform into traveling waves in the moving frame, we recorded the time dependence of u for several moving points and constructed a space-time plot. When v_x is far from the critical velocity of the T-NT transition, v_{cr} [Fig. 7(a)], waves propagate from the front edge to the rear edge of the mask with velocity about v_x and wavelength about λ_T. However, if v_x-v_{cr} is small [Fig. 7(b)], there is no single velocity of propagation. Turing peaks reside near some special point for a relatively long period of time and then a new peak emerges as an old one rapidly

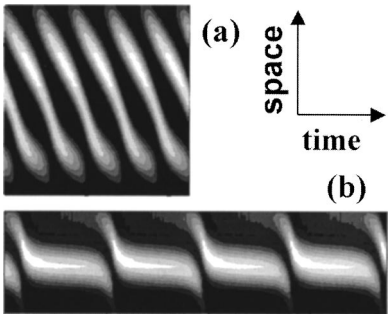

FIG. 7. Time-space plots in the moving frame for $w_1=5.2$ and (a) $l_m=8.1$, $v_x=0.5$, (b) $l_m=4.5$, $v_x=0.162$ with white corresponding to the maximum (4.32) of u and black to the minimum (0.69). Vertical space axis runs (a) from $r_0-3l_m/16$ to r_0+l_m, (b) from $r_0-3l_m/10$ to r_0+l_m; r_0 corresponds to rear edge of the moving mask. Horizontal axis is time; total interval $\Delta t=$(a) 45 and (b) 300.

disappears. The dependence of T on (v_x-v_{cr}) in the vicinity of v_{cr} (see Table IV, bottom part, with v_x between $v_{cr}=0.1555$ and $v_x=0.3$) is well fitted by the expression $T=A(v_x-v_{cr})^{-\gamma}$ with critical exponent $\gamma=0.49$ close to the theoretical value 0.5 ($A=15.3$ for the parameters in Table IV).

For reaction-diffusion-convection equations containing convective terms like the $v_x\ \partial u/\partial r$ term introduced by our moving frame ansatz, wave instability has been found in two-variable models [11,12], and the wave instability emerges at any positive v_x for spatially infinite (or periodic) systems, since $\mathrm{Im}(\lambda)=kv_x$. We obtain the same result for the present system with finite, but not too small, l_m ($k=\pi n/l_m, n=1,2,...; l_m>0.2\lambda_T$) and fixed value (Dirichlet) boundary conditions. In light of this result, it may appear strange that translational motion (i.e., a stationary solution of the system in the moving frame) exists at nonzero values of v_x.

To elucidate this question, first note that in the present case of a finite length system we have nonzero-flux boundary conditions, which strongly affect the onset of wave instability in the moving frame (dependence of v_{cr} on l_m and w_2). This wave instability also differs from the more commonly encountered case in that it emerges when $\mathrm{Im}(\lambda)$ becomes nonzero at already positive $\mathrm{Re}(\lambda)$, while in most reaction-diffusion equations, the wave instability occurs when $\mathrm{Re}(\lambda)$ becomes positive at nonzero $\mathrm{Im}(\lambda)$. For $v_x<v_{cr}$, we have a stationary Turing structure [$\mathrm{Im}(\lambda)=0$ and $\mathrm{Re}(\lambda)>0$ in some range of wave numbers $k>0$]. For $v_x>v_{cr}$, $\mathrm{Im}(\lambda)\neq 0$ and $\mathrm{Re}(\lambda)>0$. Thus, to analyze the stability, we must test the stability of a Turing pattern, rather than that of a homogeneous steady state, with respect to changes in v_x. This problem of nonlinear stability analysis is beyond the scope of this paper.

We have analyzed a specific model, Eqs. (1) and (2), because it is directly relevant to the CDIMA reaction, on which all experiments of this type have been conducted to date. Nevertheless, the results obtained, in particular the existence of the T-NT transition and the utility of the $v_x=0$ system for providing insight into the moving system, should apply to any system of this type. Here we suggest a general qualitative explanation for translational motion at small v_x. We think of a mask's motion as consisting of independent movements of its front and rear edges. Clearly, changes at the boundaries of the Turing pattern will affect the central region of the pattern. If we instantaneously shift the rear edge of the mask by a distance much less than λ_T toward the Turing pattern (toward the right), the Turing maxima will sequentially start to shift to the right, thus decreasing the apparent wavelength of the pattern, since the front edge is fixed. If we perform the same shift only at the front edge, the apparent Turing wavelength will increase, as the concentration maxima move toward the right, but now with the forward-most peaks moving the furthest. We may say that the small shift of the rear (front) edge pushes (pulls) the Turing peaks, since the apparent Turing wavelength λ_R of a real pattern in a finite system with our boundary conditions is determined by

$$\lambda_R=l_m/n, \tag{3}$$

where λ_R is the closest value to $\lambda_T=2\pi/k_0$ for some integer n. When both edges move simultaneously, we have translational motion. If the displacement of the rear (front) edge is much larger, of the order of $p\lambda_T$, with $p\approx 1$, the leftmost (a new) Turing peak disappears (emerges), thus resulting in nontranslational motion.

Let us assume that a small perturbation at the boundary propagates through a Turing pattern with some characteristic velocity v_p or time $\tau_p=l_m/v_p$. Our simulations suggest that the critical value of p, p_{cr}, at which new (old) peaks begin to appear (fade) is between 0.3 and 0.45, depending somewhat on l_m/λ_T. The critical time for mask movement is thus the time required for the mask to travel the critical distance $p_{cr}\lambda_T$, or $\tau_{cr}=p_{cr}\lambda_T/v_x$. Equating τ_{cr} and τ_p, we obtain the critical velocity $v_{cr}=p_{cr}\lambda_T/\tau_p$, for the T-NT transition. In other words, we find nontranslational or translational motion according to whether the mask moves faster or more slowly, respectively, than $v_p(p_{cr}\lambda_T/l_m)$, i.e., than a fraction $p_{cr}\lambda_T/l_m$ (which decreases with the size of the mask) of the rate at which a perturbation propagates through the Turing pattern (this velocity is smaller than the velocity of Turing patterns spreading into the homogeneous medium).

Expression (3) for λ_R allows us to estimate the variability of the apparent Turing wavelength, i.e., the effect of variable, finite size, as $|\lambda_T-\lambda_R|\cong p_{cr}\lambda_T/n$, where $p_{cr}\cong 0.5$ and $n\cong l_m/\lambda_T$, so $|\lambda_T-\lambda_R|\cong p_{cr}\lambda_T^2/l_m$. If the T-NT transition is associated with this variability of λ_R, then this estimate gives the correct dependence of v_{cr} on l_m.

V. DISCUSSION AND CONCLUSION

We have found several types of moving Turing patterns, which may be divided into two classes: translational and nontranslational. The T-NT transition, which depends upon the mask width and the light intensity beyond the mask, is connected with the onset of a wave instability in the moving frame. The transition from nontranslational motion to translational unstructured stripe motion is related to the velocity of pattern expansion in a uniform medium.

Our initial motivation for this work came from dash waves in the BZ-AOT system [1]. Returning to dash waves and taking into account that translational motion of spotlike Turing structures (the analog of dashes) occurs only at small v_x, we infer that dash waves should be associated with relatively slow trigger waves. In fact, the velocity of trigger waves in the BZ-AOT system (2–10 μm/s) [13], where the dash waves appear, is considerably smaller than in the BZ system in aqueous solution (40–100 μm/s) [14].

We have studied the behavior of Turing patterns only for the movement of a one-stripe mask. Our results may serve as a basis for analysis of interaction between Turing patterns and moving multiple-stripe masks, occupying an entire area. Preliminary studies with multiple-stripe masks reveal that there are at least three types of motion: translational motion for small v_x, nontranslational motion for intermediate v_x, and *oscillatory* patterns, which undergo small amplitude motion around their fixed positions, for large v_x. The last type of pattern arises from interactions between Turing structures in neighboring ''dark'' stripes.

We have considered the simplest case, in which no Hopf instability is present. However, in the CDIMA reaction [model (1) (2)], there are many parameter sets for which Turing and Hopf instabilities coexist. Interaction or resonance between the intrinsic frequency of oscillatory behavior associated with the Hopf instability and the translational frequency v_x/l_m or v_x/λ_T may lead to additional phenomena and patterns.

It is not difficult to envision biological systems in which the problem examined here may be relevant. One such example is the flow of blood and emergence of a clot in response to a cut. A detailed model of blood coagulation yields complex stationary spatial patterns (clots) if a capillary is perturbed locally [15]. Turing patterns have been suggested to play a significant role in morphogenesis [16]. Waves of biological activity and fronts of proliferating cells may interact with Turing patterns, creating patterns resembling those seen here.

ACKNOWLEDGMENTS

This work was supported by the Chemistry Division of the National Science Foundation. We thank Milos Dolnik for a critical reading of the manuscript.

[1] V. K. Vanag and I. R. Epstein, Phys. Rev. Lett. **90**, 098301 (2003).
[2] S. Rüdiger, D. G. Miguez, A. P. Muñuzuri, F. Sagués, and J. Casademunt, Phys. Rev. Lett. **90**, 128301 (2003).
[3] A. Horváth, M. Dolnik, A. Muñuzuri, A. M. Zhabotinsky, and I. R. Epstein, Phys. Rev. Lett. **83**, 2950 (1999).
[4] M. Dolnik, I. Berenstein, A. M. Zhabotinsky, and I. R. Epstein, Phys. Rev. Lett. **87**, 238301 (2001).
[5] M. Dolnik, A. M. Zhabotinsky, and I. R. Epstein, Phys. Rev. E **63**, 026101 (2001).
[6] M. Kaern, R. Satnoianu, A. Muñuzuri, and M. Menzinger, Phys. Chem. Chem. Phys. **4**, 1315 (2002).
[7] I. Lengyel and I. R. Epstein, Science **251**, 650 (1991).
[8] Computer code FLEXPDE, http://www.pdesolutions.com/flexpde.htm, 2001.
[9] In some experiments, it may be more convenient to vary w_2 while holding w_1+w_2 constant. The effect is the same.
[10] O. Jensen, V. O. Pannbacker, E. Mosekilde, G. Dewel, and P. Borckmans, Phys. Rev. E **50**, 736 (1994).
[11] S. P. Kuznetsov, E. Mosekilde, G. Dewel, and P. Borckmans, J. Chem. Phys. **106**, 7609 (1997).
[12] A. B. Rovinsky and M. Menzinger, Phys. Rev. Lett. **69**, 1193 (1992).
[13] V. K. Vanag and I. R. Epstein, Phys. Rev. Lett. **87**, 228301 (2001).
[14] I. R. Epstein and J. A. Pojman, *An Introduction to Nonlinear Chemical Dynamics* (Oxford University Press, New York, 1998).
[15] F. I. Ataullakhanov, V. I. Zarnitsyna, A. Y. Kondratovich, E. S. Lobanova, and V. I. Sarbash, Phys. Usp. **45**, 619 (2002).
[16] A. M. Turing, Philos. Trans. R. Soc. London, Ser. B **237**, 37 (1952).